Far-Field Control of Radiation from an Individual Optical Nanocavity: Analogue to an Optical Dipole

Jacob T. Robinson and Michal Lipson

Department of Electrical and Computer Engineering, Cornell University, Ithaca, New York 14853, USA

(Received 11 July 2007; revised manuscript received 2 November 2007; published 29 January 2008)

We demonstrate long-range control of the radiative lifetime of a silicon optical nanocavity using a metallic atomic force microscope probe. We extract changes in the radiative lifetime from changes in the cavity's transmittivity resulting from probe-cavity interaction over distances of several optical wavelengths. Analogous to atomic systems, the cavity acts as an individual radiating dipole with a radiative rate that is modified by a metallic interface.

DOI: 10.1103/PhysRevLett.100.043902 PACS numbers: 42.60.Da, 32.70.Cs, 68.37.Uv

Controlling the time that photons remain trapped in an individual state before being emitted is a fundamental challenge in photonics and quantum information processing. Optical resonant cavities allow one to trap photons for a period of time (photon lifetime) dictated by the cavity geometry. The photon lifetime (τ_p) can depend on several factors including the radiation of the cavity into free space. In active photonic devices such as switches, modulators, and buffers, it is often necessary to dynamically modify τ_p of optical resonant cavities [1]. Several techniques have demonstrated this dynamic control of τ_p. These techniques including free carrier injection [2], thermal control [3], integrated fluidics [4], and near-field probes [5] all rely on physical changes within the near field of the cavity (distances less than one wavelength).

In instances where physical modifications in the near field are impractical, far-field control of the radiative properties can in principle be achieved by manipulating the local density of states at the source. It has been known for more than three decades that reflections at metallic or dielectric interfaces can modify the local density of states for optical dipoles resulting in a change of their radiative rate [6]. While far-field control of radiative lifetimes has been observed in atomic and molecular ensembles [7–9], only recently has this been achieved for individual optical dipoles using sensitive scanned probe experiments [10]. Here, applying similar techniques, we show the first far-field control of the radiative lifetime (τ_{rad}) of an individual optical nanocavity and show it to be analogous to an individual radiating dipole.

To demonstrate far-field tuning of τ_{rad} of an optical nanocavity, we perturb the local density of states with a scanning metallic probe and extract the resulting change in τ_{rad} from the cavity's transmission properties. The effect of changing local density of states can be calculated by considering the interference between the source field and its reflection [11,12]. An increase or decrease in the local density of states is equivalent to the reflected field constructively or destructively interfering with the source field. This results in a change in τ_{rad}, which depends on the phase relationship between the source field and the radiation reflected by a metallic probe. By controlling the position of a scanning probe we tune this phase relationship, thereby controllably increasing or decreasing τ_{rad}. We increase the sensitivity of the experiment by working in a cavity configuration and extracting changes in τ_{rad} from changes in the cavity transmission. Using this technique, we can detect lifetime modifications of less than 1%. This corresponds to a temporal sensitivity of less than one femtosecond for the cavity used in our experiment, which has a τ_p of about 20 fs. Our experiment is enabled by recent development of sensitive transmission measurements similar to those made with transmission-based near-field scanning optical microscopy (TraNSOM) [13] as well as integrated resonant cavities with nanoscale mode volumes [14].

The optical nanocavity used in our experiment is embedded in a quasi-1D photonic crystal coupled to an input and output waveguide [14]. The device is fabricated in silicon on insulator using electron beam lithography and reactive ion etching. Fabrication details can be found in [13]. As seen in the scanning electron micrograph (SEM) in the Fig. 1(a) inset, the nanocavity is defined by the two sets of holes separated by about 500 nm. These sets of holes act as quasi-1D photonic crystals forming partial reflectors that trap light between them when the input wavelength matches the resonance condition [15]. The slot in the cavity center decreases the effective volume of the resonance cavity and increases the radiative rate as a result of the lower index contrast between the cavity and the cladding [16]. The experimental setup described in detail in [13] consists of amplified spontaneous emission from an erbium doped fiber amplifier filtered to $\lambda = 1565$ nm to match the cavity resonance and is coupled into and out of the device through optical fibers. The device is then imaged using a PtIr-coated probe in tapping mode on an atomic force microscope (AFM), which simultaneously records the topography and power transmitted through the device. Note that the transmission is not demodulated at the tapping frequency. In tapping mode the amplitude of probe oscillation in the z direction is about 100th of the optical wavelength used in this experiment.

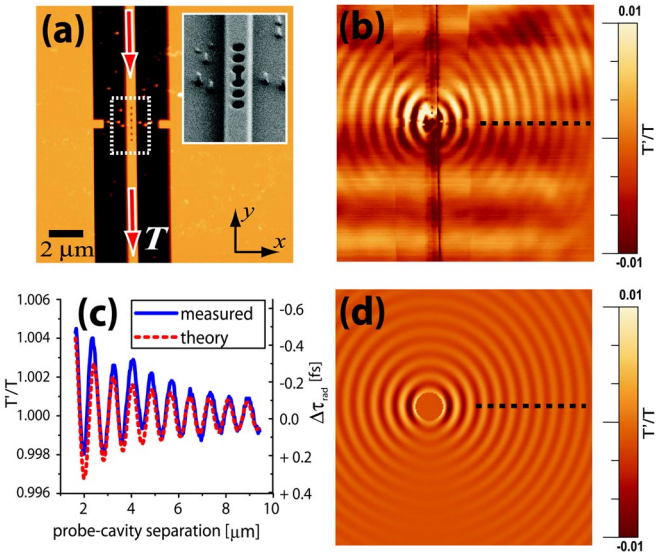

FIG. 1 (color online). (a) Topography of the resonant cavity as measured by an atomic force microscope. Inset shows a scanning electron micrograph corresponding to the dashed box. Arrows show the direction of light propagation. (b) Measured transmission through the cavity recorded simultaneously with the topography in (a). (c) Measured (solid line) and calculated (dashed line) relative change in transmission (T'/T) and corresponding change in radiative lifetime ($\Delta\tau_{\mathrm{rad}}$) as a function of the source-probe separation taken along the dashed lines in (b) and (d), respectively. (d) Calculated change in transmission as a function of probe position based on the model in Fig. 2.

Therefore, the effect of probe oscillation on the change in radiative lifetime is negligible and the probe can be considered to be in contact with the surface. Figure 1(a) shows the topography of the resonant cavity as measured with the AFM, and Fig. 1(b) shows the simultaneously measured change in transmission as a function of probe position. Figure 1(c) shows a cross section through the measured data and theoretical model taken along the dashed line in Figs. 1(b) and 1(d), respectively. Figure 1(d) represents a theoretical model for the experimentally measured change in transmission shown in Fig. 1(b). This model, based on probe-cavity interaction, is explained in detail in the following sections.

To extract the change in τ_{rad} from the measured change in power transmitted through the cavity, we model the optical cavity as shown in Fig. 2(a). We can write the on-resonance cavity transmittivity (T) and reflectivity (R) of the cavity shown in Fig. 2(a) as [17]

$$T = [(2/\tau_c)/(1/\tau_{\mathrm{rad}} + 2/\tau_c)]^2, \tag{1}$$

$$R = [(1/\tau_{\mathrm{rad}})/(1/\tau_{\mathrm{rad}} + 2/\tau_c)]^2, \tag{2}$$

where τ_{rad} and τ_c are the radiative and coupling lifetimes, respectively. Since absorption in small volume resonant cavities is negligible [18], τ_{rad} refers to the time it takes for the energy in the resonant cavity to decay by a factor of $1/e$ if the cavity is isolated from the input and output waveguides. Similar to atomic dipoles, the stored energy is lost by radiation into free space that is determined by the local density of states. The coupling lifetime, on the other hand, refers to the time it takes light to couple into or out of the resonant cavity through the waveguides [Fig. 2(a)]. It is important to note that, unlike τ_{rad}, τ_c is independent of the local density of states and is determined only by the mode overlap between the guided mode in the resonator, the decaying Bloc mode in the 1D photonic crystal, and the waveguide mode [18]. Since the probe is several wavelengths away from the guided modes, we can apply first order perturbation theory and assume that the mode profiles do not change as a result of the probe [19] and the overlap integrals that determine τ_c remain unchanged. The photon lifetime refers to the time it takes the energy in the coupled cavity [Fig. 2(a)] to decay by a factor of $1/e$ and can be written as $1/\tau_p = 1/\tau_{\mathrm{rad}} + 2/\tau_c$. Defining the ratio of the unperturbed radiative to coupling lifetimes as $\beta \equiv \tau_{\mathrm{rad}}/\tau_c$, we can write the relative change in transmission in terms of the change in τ_{rad}:

$$\frac{T'}{T} = \left[\frac{\tau_p'}{\tau_p}\right]^2 = \left[\frac{1+2\beta}{\tau_{\mathrm{rad}}/\tau_{\mathrm{rad}}' + 2\beta}\right]^2. \tag{3}$$

Here the primes indicate the perturbed quantities. In principle β can be determined experimentally from the ratio of the on-resonance transmittivity (1) and reflectivity (2) of the resonator: $\beta = 1/2\sqrt{T/R}$ [17]. In practice this requires precise knowledge of the transmission and reflection coefficients at each optical fiber-to-chip interface. Since the positions of the optical fibers shift slightly during the adhesive curing process, the coefficients at these interfaces vary significantly, making the absolute transmission properties difficult to characterize. Instead, we estimate β by

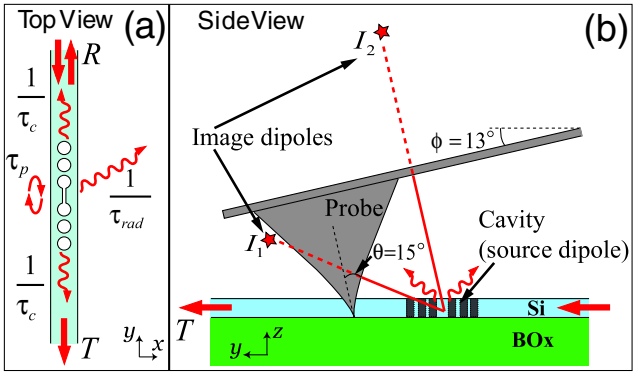

FIG. 2 (color online). (a) Schematic of an optical resonant cavity coupled to the input and output waveguides where T and R are the transmittivity and reflectivity, respectively. (b) Model of the cavity-probe interaction as viewed from the side (not to scale). Stars labeled I_1 and I_2 represent image dipoles resulting from reflections at the probe apex and cantilever, respectively.

simulating pulse propagation through the device using a 3D finite difference time domain method. Using this technique we calculate an on-resonance transmittivity of $T = 0.48$ and reflectivity of $R = 0.10$ from which we estimate β to be 1.10. Note that we neglect the transmission change resulting from a shift in resonant frequency since for classical dipoles this effect is smaller than the change in τ_{rad} by a factor $1/\omega_0\tau_{\mathrm{rad}} \ll 1$ [12]. Note that in Fig. 1(b) changes in τ_{rad} are observed at distances of more than nine microns from the source, which corresponds to more than five optical wavelengths. This confirms we are indeed observing source-probe interaction beyond the near field.

The oscillation of the transmitted power shown in Figs. 1(b)–1(d) can be understood by the model shown in Fig. 2(b) depicting a side view of the cavity and the image dipoles resulting from the reflections by the probe. Reflection from the tip of the probe and the cantilever create two distinct image dipoles denoted as the stars labeled I_1 and I_2, respectively. As the probe position changes, the distances between the source and image dipoles change, altering the phase relationship between the source and reflected fields. Therefore, we expect τ_{rad} to oscillate as a function of the probe position, which we indeed measure in Fig. 1(b). Based on the geometry of the probe-cavity interaction in Fig. 2(b), we expect the lifetime oscillation due to I_1 to have a period of $\lambda/2\cos(\theta)$ where θ is the half-angle of the probe cone near the apex as depicted in Fig. 2(b). Since θ is a small angle ($15° \pm 3°$ according to SEM images of the probe) the period of the oscillation is close to half the free space wavelength (0.783 microns). This corresponds to the dipolelike radiation pattern centered at the cavity as shown in Fig. 1(b). On the other hand, lifetime oscillation due to I_2 should have a period of $\lambda/2\sin(\phi)$ where ϕ is the angle of the cantilever that is specified by the manufacturer to be $13° \pm 0.5°$. This corresponds to a period of about 7 microns and should vary only as the probe is scanned in the y direction. This is seen as the long oscillations along the y direction measured in Fig. 1(b). Note that a scan along the y direction corresponds to a scan from right to left in Fig. 2(b) and a scan from bottom to top in Fig. 1(b). We verify the effect of both image dipoles by plotting in Fig. 3 the 2D fast Fourier transform (2DFFT) of Fig. 1(b). Indeed, Fig. 3 shows distinct peaks at large wave numbers near $4\pi\cos(15°)/\lambda$ (dotted circle) as well as peaks at small wave numbers along the y direction near $4\pi\sin(13°)/\lambda$ (dashed lines). Note that the probe is modeled simply as a reflecting surface at an angle determined according to Fig. 2(b) and a reflectivity that contributes to the constant κ defined below. Probes of other materials or complex geometries with multiple facets could allow for additional image dipoles of varying magnitudes that could result in a greater overall effect on τ_{rad}.

To quantify the absolute change in τ_{rad}, we mathematically express the above model and compare it to the

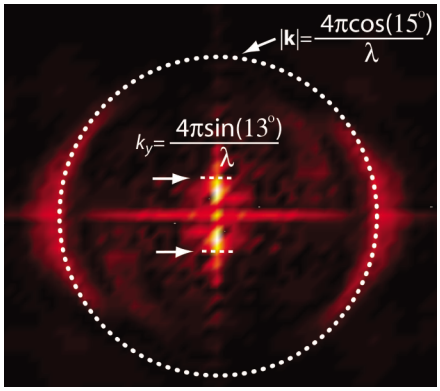

FIG. 3 (color online). A 2DFFT of the data in Fig. 1(b). Dotted circle shows the wave numbers corresponding to the probe cone half-angle of 15°. Dashed line shows the wave numbers along the y direction corresponding to the cantilever angle of 13°.

measured data using a single fitting parameter. The field from the image dipoles interacts with the cavity (source dipole) perturbing its dipole moment. We write this perturbed dipole moment ($\mathbf{p}'$) as the sum of the unperturbed dipole moment ($\mathbf{p}$) and the effect of the image dipole: $\mathbf{p}' = \mathbf{p} - \kappa|\mathbf{p}|\mathbf{e}_p(\mathbf{r})$. Here the image dipole is represented as $|\mathbf{p}|\mathbf{e}_p(\mathbf{r})$ where $\mathbf{e}_p(\mathbf{r})$ is the electric field of a unit dipole at position $\mathbf{r}$ [determined by the probe position according to Fig. 2(b)] measured at the cavity position. This term is multiplied by the reflectivity of the probe and the effective polarizability of the cavity, which we group as a single term κ that is our fitting parameter. Note from the minus sign preceding $\mathbf{e}_p$ that we have assumed that reflection from the metallic probe results in a π phase shift as expected from near-perfect metals. Since the radiated power is proportional to the square of the oscillating dipole moment [12], we can write

$$\tau_{\mathrm{rad}}/\tau'_{\mathrm{rad}} = |\mathbf{p}'|^2/|\mathbf{p}|^2 = |\hat{\mathbf{p}} - \kappa\mathbf{e}_p(\mathbf{r})|^2. \quad (4)$$

We calculate the expected change in transmission as a function of probe position by first calculating the known radiation pattern of a unit dipole, combining (4) with (3), and taking the unit vector $\hat{\mathbf{p}}$ to be along the y direction [as suggested by Fig. 1(b)], and β to be the calculated value of 1.09. We then fit our model to the measured data using a least-squares fit along the dashed line in Fig. 1(b) with κ as the sole fitting parameter. According to the fit, we determine $\kappa = 4\pi\varepsilon_0(6.3 \pm 0.1 \times 10^{-22})$ m^3 (which is about 8 orders of magnitude larger than the polarizability of a single atom) and plot our model (dashed line) and the measured data (solid line) in Fig. 1(c). Note we have applied this fit over a region where the probe is more than one wavelength away from the cavity center. This is done to avoid probe-cavity interactions in the near field where the analogy between the nanocavity and a radiating dipole breaks down since one must consider the exact mode profile of the resonant cavity [20,21]. The model

shows excellent agreement with the measured data for large probe-cavity separations. For short separation distances, however, the measured data have a slightly longer oscillation period since the half-cone angle of the probe is smaller near the apex. We determine the unperturbed value of τ_{rad} from the full width half maximum (FWHM) of the resonance ($\Delta\lambda = 65 \pm 12$ nm) and the calculated value of β according to $\tau_{\mathrm{rad}} = (1 + 2\beta)\lambda_0^2/2\pi c\Delta\lambda = 64 \pm 13$ fs. This can be derived from the definition of β and $\omega_0\tau_p \approx \lambda/\Delta\lambda$ [19]. Using the values of $\beta = 1.10$ and $\tau_{\mathrm{rad}} = 64$ fs, we calculate the absolute change in τ_{rad} according to (1) and represent those values as the y axis on the right hand side of Fig. 1(c). Note that by extracting the change in τ_{rad} from the change in transmission we are able to resolve changes of less than one femtosecond, which would be extremely difficult to measure in the time domain. For high-Q cavities, however, such as those reported in [22], this long-range change in τ_{rad} could be on the order of picoseconds. Optimizing the probe geometry could also greatly enhance these long-range effects.

To verify that our model correctly predicts the measured transmission changes in two dimensions [Fig. 1(b)], we plot in Fig. 1(d) the simulated 2D probe-cavity interaction based on (1), the calculated value of β, and the fitted parameter κ. Note that in Fig. 1(d) we have included only the effect of the image dipole formed by the probe [I_1 in Fig. 2(b)] since this is the most sensitive to the probe position. We see that the simulated transmission changes in Fig. 1(d) indeed match the measured dipolelike pattern shown in Fig. 1(b). Note that Fig. 1(d) is generated based on the angle of both the probe and the cantilever as shown in Fig. 2(b). The small 13° angle of the cantilever causes the pattern above the cavity (positive y) to be slightly different from the pattern below the cavity (negative y). Although this effect is small, the fringes above the cavity are noticeably stronger than those below the cavity in both the measured [Fig. 1(b)] and calculated [Fig. 1(d)] images.

By controlling the position of a scanning probe in the optical far-field, we have demonstrated the first far-field control of the radiative lifetime of an individual optical nanocavity. By extracting this change in τ_{rad} from the change in resonant cavity transmission, we have demonstrated subfemtosecond temporal sensitivity. Although the magnitude of change in τ_{rad} reported in this Letter is less than 1%, these changes can be extremely precise and tunable. The magnitude can be increased by changing the reflectivity of the probe material or altering the geometry to allow for a greater number of image dipoles. The long-range control of radiative properties reported here could lead to advances in photonics and quantum information processing, which require precise control over photon dynamics. We have also shown that radiation from photonic nanocavities is analogous to individual optical dipole radiation. This opens the door to new experiments controlling and characterizing the radiation properties of individual optical dipoles as well as photonic nanocavities.

Research support is gratefully acknowledged from the NSF CMDITR, No. DMR-0120967, the Cornell Center for Material Research, the NSF's CAREER Grant No. 0446571, and the U.S. Air Force MURI program on "Electrically-Pumped Silicon-Based Lasers for Chip-Scale Nanophotonic Systems." This work was performed in part at the Cornell NanoScale Facility, a member of the NNIN, which is supported by the NSF (Grant No. ECS 03-35765), and we made use of STC shared experimental facilities supported by the NSF under Agreement No. ECS-9876771.

[1] M. Lipson, J. Lightwave Technol. **23**, 4222 (2005).
[2] V. R. Almeida, C. A. Barrios, R. R. Panepucci, and M. Lipson, Nature (London) **431**, 1081 (2004).
[3] H. M. H. Chong and R. M. D. L. Rue, IEEE Photonics Technol. Lett. **16**, 1528 (2004).
[4] U. Levy, K. Campbell, A. Groisman, S. Mookherjea, and Y. Fainman, Appl. Phys. Lett. **88**, 111107 (2006).
[5] I. Marki, M. Salt, and H. P. Herzig, Opt. Express **14**, 2969 (2006).
[6] K. H. Drexhage, M. Fleck, H. Kuhn, F. P. Schäfer, and W. Sperling, Ber. Bunsen-Ges. Phys. Chem. **70**, 1179 (1966).
[7] E. Snoeks, A. Lagendijk, and A. Polman, Phys. Rev. Lett. **74**, 2459 (1995).
[8] R. M. Amos and W. L. Barnes, Phys. Rev. B **55**, 7249 (1997).
[9] J.-Y. Zhang, X.-Y. Wang, and M. Xiao, Opt. Lett. **27**, 1253 (2002).
[10] B. C. Buchler, T. Kalkbrenner, C. Hettich, and V. Sandoghdar, Phys. Rev. Lett. **95**, 063003 (2005).
[11] R. R. Chance, A. Prock, and R. Silbey, J. Chem. Phys. **60**, 2744 (1974).
[12] J. D. Jackson, *Classical Electrodynamics* (J. Wiley & Sons, Inc., Hoboken, NJ, 1999), 3rd ed.
[13] J. T. Robinson, S. F. Preble, and M. Lipson, Opt. Express **14**, 10588 (2006).
[14] J. T. Robinson, C. Manolatou, L. Chen, and M. Lipson, Phys. Rev. Lett. **95**, 143901 (2005).
[15] J. S. Foresi, P. R. Villeneuve, J. Ferrera, E. R. Thoen, G. Steinmeyer, S. Fan, J. D. Joannopoulos, L. C. Kimerling, H. I. Smith, and E. Ippen, Nature (London) **390**, 143 (1997).
[16] V. R. Almeida, Q. Xu, C. A. Barrios, and M. Lipson, Opt. Lett. **29**, 1209 (2004).
[17] H. A. Haus and Y. Lai, IEEE J. Quantum Electron. **28**, 205 (1992).
[18] C. Sauvan, G. Lecamp, P. Lalanne, and J. Hugonin, Opt. Express **13**, 245 (2005).
[19] L. A. Coldren and S. W. Corzine, *Diode Lasers and Photonic Integrated Circuits* (J. Wiley & Sons, Inc., New York, 1995).
[20] A. F. Koenderink, M. Kafesaki, B. C. Buchler, and V. Sandoghdar, Phys. Rev. Lett. **95**, 153904 (2005).
[21] W. C. L. Hopman, R. Stoffer, and R. M. d. Ridder, J. Lightwave Technol. **25**, 1811 (2007).
[22] B.-S. Song, S. Noda, T. Asano, and Y. Akahane, Nat. Mater. **4**, 207 (2005).